Role of the bridging group in bis-pyridyl ligands: enhancing both the photo- and electroluminescent features of cationic (IPr)Cu I complexes

Margaux Elie, Michael D. Weber, Florent Di Meo, Fabien Sguerra, Jean-François Lohier, Robert B. Pansu, Jean-Luc Renaud, Matthieu Hamel, Mathieu Linares, Rubén D. Costa, et al.

▶ **To cite this version:**

Margaux Elie, Michael D. Weber, Florent Di Meo, Fabien Sguerra, Jean-François Lohier, et al.. Role of the bridging group in bis-pyridyl ligands: enhancing both the photo- and electroluminescent features of cationic (IPr)Cu I complexes. Chemistry - A European Journal, 2017, 23 (64), pp.16328-16337. 10.1002/chem.201703270 . hal-01633172

HAL Id: hal-01633172
https://hal.science/hal-01633172v1

Submitted on 12 Jan 2023

HAL is a multi-disciplinary open access archive for the deposit and dissemination of scientific research documents, whether they are published or not. The documents may come from teaching and research institutions in France or abroad, or from public or private research centers.

L'archive ouverte pluridisciplinaire **HAL**, est destinée au dépôt et à la diffusion de documents scientifiques de niveau recherche, publiés ou non, émanant des établissements d'enseignement et de recherche français ou étrangers, des laboratoires publics ou privés.

Role of the Bridging Group in Bis-Pyridyl Ligands: Enhancing Both the Photo- and Electroluminescent Features of Cationic $(IPr)Cu^{I}$ Complexes

Margaux Elie[a], Michael D. Weber[b], Dr. Florent Di Meo[c], Dr. Fabien Sguerra[e], Jean-François Lohier[a], Dr. Robert B. Pansu[f], Prof. Jean-Luc Renaud[a], Dr. Matthieu Hamel[e], Dr. Mathieu Linares[d,g], Dr. Rubén D. Costa[b,h], Dr. Sylvain Gaillard[a]

a Normandie University, LCMT, ENSICAEN, UNICAEN, CNRS 14000, Caen (France) E-mail:sylvain.gaillard@ensicaen.fr
b Department of Chemistry and Pharmacy, University of Erlangen-Nuremberg, Egerlandstr. 3, 91058 Erlangen (Germany)
c INSERM UMR 850, Univ. Limoges, Faculty of Pharmacy, 2 rue du Dr. Marcland, 87025 Limoges (France)
d Division of Theoretical Chemistry and Biology, School of Biotechnology, KTH Royal Institute of Technology, 106 91 Stockholm (Sweden) E-mail:linares@kth.se
e CEA, LIST, Laboratoire Capteurs et Architectures Électroniques, 91191 Gif-sur-Yvette Cedex (France)
f PPSM, CNRS, UMR 8531 & Inst. d'Alembert FR3242, ENS Cachan, Paris Saclay University (France)
g IMDEA Materials, C/ Eric Kandel, 2, Tecnogetafe, 28906, Getafe, Madrid (Spain) E-mail:ruben.costa@imdea.org

Abstract

We report on the benefits of changing the bridging group X of bis-pyridyl ligands, that is, Py-X-Py where X is NH, CH_2, $C(CH_3)_2$, or PPh, on the photo- and electroluminescent properties of a new family of luminescent cationic H-heterocyclic carbene (NHC) copper(I) complexes. A joint experimental and theoretical study demonstrates that the bridging group affects the molecular conformation from a planar-like structure (X is NH and CH_2) to a boat-like structure (X is $C(CH_3)_2$ and PPh), leading to i) four-fold enhancement of the photoluminescence quantum yield (ϕ_{em}) without affecting the thermally activated delayed fluorescence mechanism, and ii) one order of magnitude reduction of the ionic conductivity (σ) of thin films. This leads to an overall enhancement of the device efficacy and luminance owing to the increased ϕ_{em} and the use of low applied driving currents.

1 Introduction

Significant attention has recently been devoted to the development of new organic or organometallic emitters for solid-state lighting technologies. In this field, a leading example is light-emitting electrochemical cells (LECs) owing to their simpler architecture compared with organic light-emitting diodes (OLEDs)[1]. Indeed, the presence of ions in the active layer makes the use of charge transport and injection layers unnecessary. Up to now, one of the most successful families of LEC is that with active layers based on ionic transition noble metal complexes, such as iridium(III) and/or ruthenium(II). Despite the excellent device performance with respect to stability and efficiency, these types of emitters rely on rare metals, whose resources are not sustainable for large-scale device production. Consequently, researchers have turned their attention to less expensive transition-metal complexes, with copper(I) as a frontrunner [2]. One of the advantages of using copper(I) complexes [3] is their unique emission mechanism based on a singlet harvesting process through thermally activated delayed fluorescence (TADF) [4]. Since the pioneering work of McMillin and co-workers [5], many homoleptic and heteroleptic complexes with two bidentate diiminine and diphosphine ligands have been studied. The main drawback of this family is the flattening process in the excited state that promotes efficient ligand exchange [6, 7] To circumvent this issue, a few new families of copper(I) complexes have recently emerged, namely i) cationic dinuclear copper(I) complex bearing

tripodal phosphine and 4,4′-bipyridine bridging ligands [8], ii) cationic copper(I) with tripodal based pyridine and monophosphine ligands [9], and iii) cationic dinuclear copper(I) complexes bearing 3-(2′-pyridyl)pyrazole and two diphosphine ligands bridging the two metal centers [10]. Recently, N-heterocyclic carbenes (NHCs), which are known as bulky and metal stabilizing ligands [11], have been envisaged for the development of new luminescent cationic copper(I) complexes [12]. Among these cationic NHC copper(I) complexes, we [13] and others [14] have reported cationic three-coordinated copper(I) complexes, in which the "N^N ligand" was a six-membered ring chelate with two pyridine rings and a borate [14] or an amine [13] as bridging group. In our previous studies, we reported a blue-emitting [Cu(IPr)(dpa)][PF_6] complex **1** (IPr = 1,3-bis (2,6-diisopropylphenyl) imidazol-2-ylidene, dpa = di (2-pyridyl)amine) [13a] and its application in LECs [13c]. Here, we have identified key structural and electronic parameters that clearly affect the photoluminescence features of this novel family of compounds. In a few words, the dpa ligand leads to a non-coplanar geometry between the diamine ligand and the imidazole ring of the NHC [13a]. The photoluminescence properties can also be modified by attaching electron-donating and/or -accepting groups at the periphery of the dpa ligand [13c].

Indeed, the excellent photoluminescence features of NHC copper(I) complexes compared with those derived from McMillin's works seems to be related to a significant breaking of the molecular symmetry towards an extended Y-shape geometry [16], compared with the tetrahedral one. The 2,2′-bis-pyridyl derivatives are six-membered chelates, in contrast to the most commonly encountered five-membered ring chelate ligands, such as 1,10-phenanthroline (phen) or 2,2′-bipyridine (bipy) [13a]. Unfortunately, LECs based on the archetypal complex **1** performed poorly, that is, with a luminance of 6 cd m^{-2} and efficacy of 0.004 cd A^{-1}, owing to the need of high applied currents (50 mA) [13c]. This scenario changes for devices with an emitter bearing a modified version of the dpa ligand, that is, luminance of 20 cd m^{-2} and efficacy of 0.22 cd A^{-1} at applied currents of 5 mA [13c].

To further provide insights on how changing the molecular structure affects both the photo- and electroluminescent features of NHC copper(I) complexes, we decided to study the role of the bridging atom. Our working hypothesis is to significantly force the molecular distortion of the dpa ligand through bridging atoms, which leads to a tetrahedral conformation of this ligand. This should promote a significant symmetry breaking, leading to enhanced photoluminescence features and, in turn, better device performance should arise.

As such, this work describes the synthesis of a new series of cationic NHC copper(I) complexes coordinated to bis-pyridyl ligands (Figure 1), with different bridging groups, such as NH (**1**), CH_2 (**2**), $C(CH_3)_2$ (**3**), or PPh (**4**). A joint experimental and theoretical study sheds light onto how structural and electronical changes related to the central atom of the bis-pyridyl ligand promote a more relevant symmetry break that significantly affects the maximum wavelength, the photoluminescence quantum yields (ϕ_{em}), and maintains the TADF emission mechanism. Finally, we also identified how the molecular changes affect the ionic conductivity (σ) of thin films, controlling the charge injection process under device operation conditions. Herein, a significant enhancement of the device luminance and efficacy reaching values of around 15 cd m^{-2} and 0.4 cd A^{-1} are reported by replacing the NH bridging atom of the archetypal complex **1** for the novel PPh bridging atom of **4**.

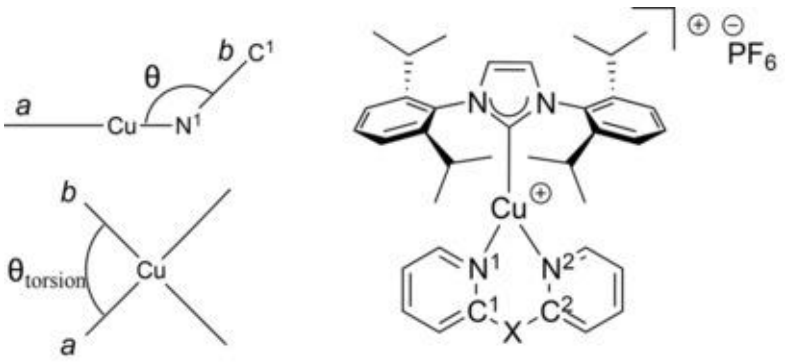

X = NH (**1**), CH_2 (**2**), $C(Me)_2$ (**3**)or PPh (**4**)

θ = plane angle

$\theta_{torsion}$ = diedral angle between planes a and b

a = plane of the imidazole ring of the NHC ligand

b = plane passing by N^1, C^1, C^2 and N^2 in the N^N ligand

bite angle is the N^1-Cu-N^2 angle

Figure 1: Definition of the plane angle θ and the torsion angle $\theta_{torsion}$.

2 Results and Discussion

2.1 Synthesis

The 2,2′-dipyridylmethane (dpym) ligand was prepared by SN_{Ar} reaction between α-picolin and 2-fluoropyridine in 78 % yield (Scheme 1) [16]. Dialkylation of dpym with iodomethane gave 2,2-(2,2′-dipyridyl)propane (dpyp) in 50 % yield (Scheme 1) [17]. Finally, 2-bromopyridine was subjected to a halogen/lithium exchange reaction and then engaged with dichlorophenylphosphine to furnish phenyl-2,2′-dipyridylphosphine ($PPhpy_2$) in 72 % isolated yield (Scheme 1) [18].

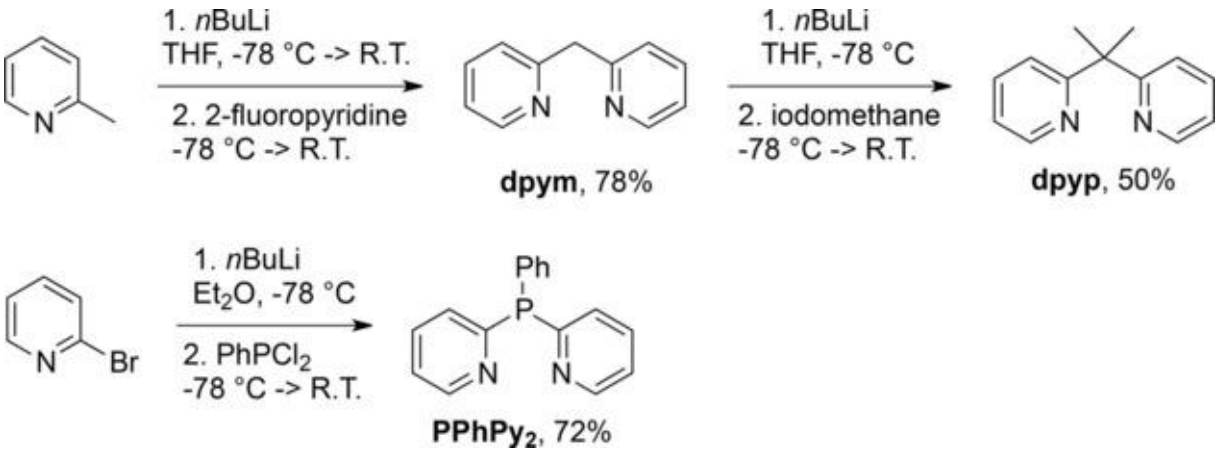

Scheme 1: Synthesis of N^N ligands with different bridging atoms.

Complex **2** was prepared according to our previously reported procedure by using [CuCl(IPr)] in 96 % isolated yield (Scheme 2) [13]. For complexes **3** and **4**, the procedure using [CuCl(IPr)] failed to provide pure complexes. Therefore, complexes **3** and **4** were synthesized by adding dpyp or $PPhpy_2$ ligands to [CuOH(IPr)] in the presence of one equivalent of $HBF_4{\cdot}OEt_2$, followed by anion metathesis using KPF_6 in methanol. Complexes **3** and **4** were obtained in 59 % and 72 % overall yield, respectively (Scheme 2) [13a, 13c].

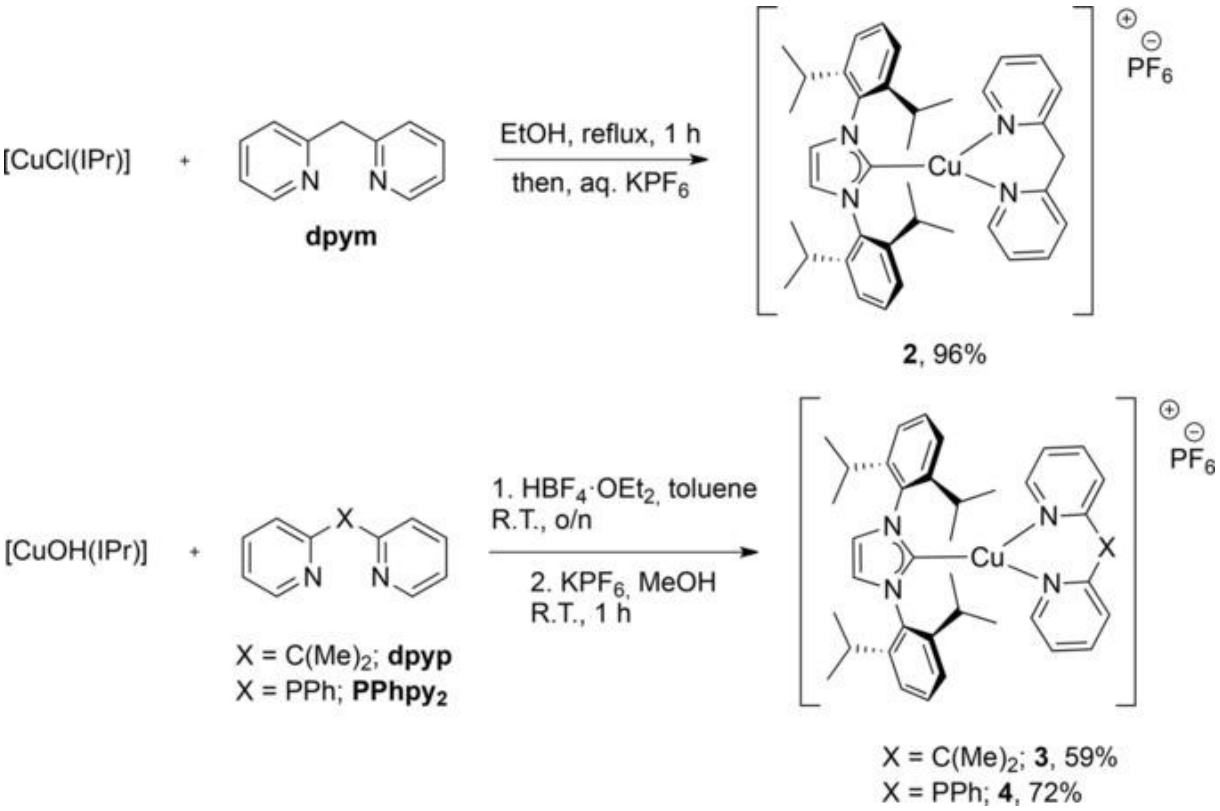

Scheme 2: Synthesis of complexes **2**–**4**.

2.2 Molecular and electronic structure study

To unambiguously establish the significance of the bridging atom on the molecular structure, single crystals were obtained and subjected to X-ray diffraction (XRD). Figure 1 defines some geometrical parameters, whereas Figure 2 displays an ellipsoid representation of the molecular structures of 1, 2, 3 a and 3 b (where 3 a features the usual coordination of the N^N ligand and 3 b shows a twisted coordination of the N^N ligand), and 4. In addition, the latter are provided along with a selection of the most relevant molecular structural parameters and photophysical properties (see below). In detail, a meaningful geometrical element is the plane angle θ between the two ligands in the copper(I) complexes previously observed as defined in [Cu(NHC)(dpa)][X] (Figure 1) [13c]. Another key parameter is the torsion angle θtorsion between the two ligands. This was previously defined by Thompson and Yersin and co-workers for NHC copper(I) complexes coordinated to dimethyldipyridylborate ligands [14b]. A direct comparison of those XRD analyses allows us to highlight four relationships between the structure and the chemical nature of the ligands. Firstly, the expected six-membered-ring coordination of both ligands in 2, 3 a, 3 b, and 4 was confirmed (Figure 2 and Figure S1 in the Supporting Information), even though the PPhpy2 ancillary ligand could also promote competitive coordination with the bridging phosphorus atom [19]. Secondly, the three new ligands dpym, dpyp, and PPhpy2 adopt a boat-like conformation in regard to the six-membered ring, including the CuI metal center (Figure 2). This leads to higher distorted conformations compared with the dpa ligand in 1 (Figure 2). This is illustrated by the values of the N1-C1···X-C2 dihedral angles: 19.9(4), 57.4(2), 63.5(2), and 63.1(1)° for complexes 1, 2, 3 a, and 4, respectively (Table 1). The boat conformation is caused by a more pronounced pyramidal geometry of the carbon and phosphorus bridging atoms. Noteworthy, the dihedral angle in dpyp in 3 is increased by around 6° compared with that noted in dpym in 2 owing to the presence of the gem-dimethyl substituent generating tetrahedral distortion by their steric hindrance and electronic repulsion, the so-called Thorpe–Ingold effect, although it is close to the one in PPhpy2 (4) [20].

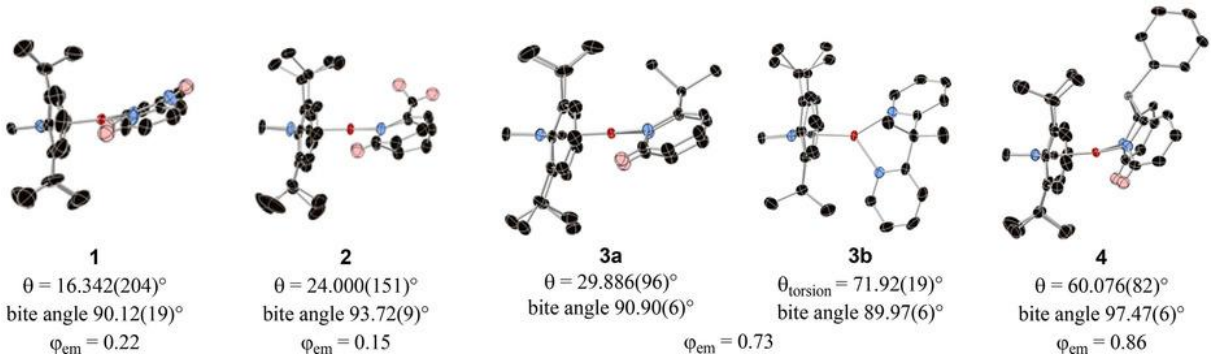

Figure 2: Ellipsoid representation of complexes **1**–**4** (lateral view exposing the plane angle θ (Figure 1). The hydrogen atoms, the anions, and the numbering have been omitted for clarity. $\theta_{torsion}$ is the torsion angle between planes a and b (Figure 1). Please refer to Figure S1 in the Supporting Information for a top view of the three-coordinated copper(I) metal center.

Entry	Complex	Cu–C_{IPr} [Å]	Cu···N [Å]	N^1···Cu···N^2 [°]	N^1-C^1···X-C^2 [°]	Plane angle θ[a] [°]	CH···Cg[b] [Å]
1	1	1.918(4)	2.040(4) 2.065(4)	90.12(19)	19.896(370)	16.342(204)	2.56 2.42
2	2	1.906(2)	2.058(2) 2.063(2)	93.72(9)	57.352(229)	24.000(151)	2.58 2.62
3	3 a	1.8985(16)	1.9859(14) 2.0495(14)	90.90(6)	63.48(18)	29.886(96)	2.66 2.61
4	3 b	1.8767(16)	2.0415(14) 2.0455(14)	89.97(6)	61.38(20)	–	none
5	4	1.8935(17)	2.0169(15) 2.0617(14)	97.47(6)	63.059(103)	60.076(82)	none

Table 1: Selected bond lengths and angles of complexes **1**–**4**.
[a] The plane angle θ is defined in Figure 1.
[b] Only CH–π interactions between the aromatic rings of IPr and the hydrogen atoms in the alpha position of the bridged dipyridyl derivative are indicated.

Another important geometry modification concerned the plane angles θ (Figure 1) in complex **4** with a value found at 60.1(1)°. θ values of 16.3(2), 24.0(2), and 29.9(1)° were found for **1**, **2**, and **3 a**, respectively (Table 1). From a structural point of view, the high θ value in **4** leads to the loss of the CH–π interactions that are usually observed between the aromatic rings of IPr and the hydrogen atoms of the bis-pyridyl derivatives. Such substantial increase in the θ value is correlated with the Cu–C_{IPr} bond lengths, which decrease in the order 1.918(4), 1.906(2), 1.899(2), and 1.894(2) Å for **1**, **2**, **3 a**, and **4**, respectively (Table 1).

The last observation came from the variation of the bite angle, which increases from 90.1(2), to 90.9(1), to 93.7(1), and to 97.5(1)° for **1**, **3 a**, **2**, and **4**, respectively (Table 1). Again, the Thorpe–Ingold effect might explain the value of the bite angle in **3 a**. This is lower than the one in **2,** but closer to that in **1** (90.1(2) vs. 90.9(1)°, Table 1).

Next, changes in the electronic structure of this family of complexes were investigated by using density functional theory (DFT) calculations. Here, the models $[Cu(IPr)(dpym)]^+$ ($\mathbf{2}^+$), $[Cu(IPr)(dpyp)]^+$ ($\mathbf{3\,a}^+$ and $\mathbf{3\,b}^+$ corresponding to the two conformers observed by XRD analysis), and $[Cu(IPr)(PPhPy_2)]^+$ ($\mathbf{4}^+$) were compared with the archetypal $[Cu(IPr)(dpa)]^+$ ($\mathbf{1}^+$; Figure 3). Common to all complexes, the HOMO is located at the Cu atom 3d and $N_{pyridyl}$ $2p_z$ orbitals, whereas the LUMO is centered on both pyridine rings (Figure 3), suggesting a strong ground-state charge-transfer (GS-CT) nature. Electron population analysis highlights, however, a weaker GS-CT in fully π-conjugated ligands, that is, $\mathbf{1}^+$ and $\mathbf{4}^+$ with respect to $\mathbf{3}^+$ and $\mathbf{2}^+$ (Table S6 in the Supporting Information). The

decrease of π-conjugation in the bis-pyridyl ligands leads to an electron enrichment in the N-Cu-(N^N) region and HOMO destabilization. Notably, the absence of π-conjugation between pyridyl moieties increases the GS-CT from both the NHC and bis-pyridyl ligand. This is associated with an increase of the electron population that strongly stabilizes the LUMO. Even though the electronic effects are different, $\mathbf{2}^+$, $\mathbf{3}^+$, and $\mathbf{4}^+$ exhibit lower HOMO–LUMO gaps than that of $\mathbf{1}^+$, due to a lower π-conjugation within only the bis-pyridyl moiety. On the one hand, $\mathbf{2}^+$ and $\mathbf{3}^+$ feature a broken π-conjugation owing to the bridging carbon atom. On the other hand, $\mathbf{4}^+$ shows a decreased bis-pyridyl π-conjugation due to the presence of an attractive phenyl moiety and the more pyramidal geometry of the phosphorus bridging atom. Hence, these findings confirm that our approach was successful with respect to the expected molecular distortions provided by the nature of the bridging atom.

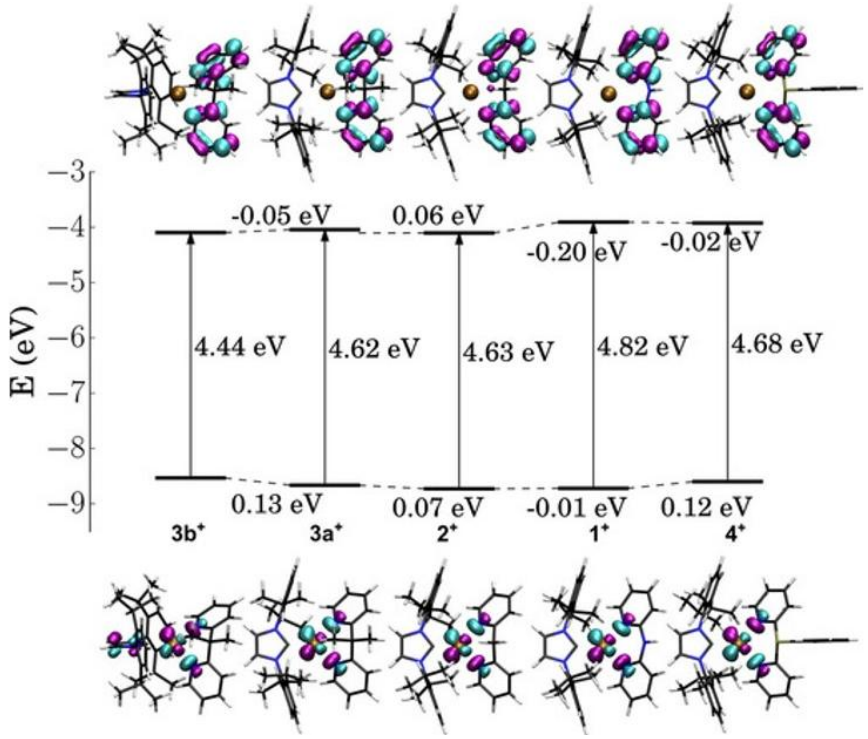

Figure 3: HOMO and LUMO distributions and energies as well as HOMO–LUMO gaps for complexes $[Cu(IPr)(dpa)]^+$ ($\mathbf{1}^+$), $[Cu(IPr)(dpym)]^+$ ($\mathbf{2}^+$), $[Cu(IPr)(dpyp)]^+$ ($\mathbf{3\,a}^+$ and $\mathbf{3\,b}^+$), and $[Cu(IPr)(PPhpy_2)]^+$ ($\mathbf{4}^+$) (isovalues: 0.005 e a_0^{-3}, $[Cu(IPr)(dpa)]^+$ ($\mathbf{1}^+$) is taken as the initial reference).

2.3 Photophysical study

The absorption spectra of 2, 3, and 4 show a first intense band assigned to a π–π* transition of the ancillary ligands between 244 and 269 nm with an additional band at 279 nm in the case of 4 (Table 2). More interesting are the shifts related to the d–π* metal-to-ligand charge-transfer (MLCT) absorption bands, which are typically influenced by changes in the molecular structure. For instance, a redshifted (10 nm) MLCT band was observed for 1 and 2 compared with that of 3, whereas a more significant redshift of around 15 nm was noted for 4 (25 nm if 3 is considered as a reference). This trend could be explained by the changes of the electron donation character related to the central atom. For instance, the lone pair of the nitrogen bridging atom is involved in the π-conjugation within both pyridine rings (see above), whereas the geometry of the phosphorus bridging atom implies that inductive effects are more important than mesomeric effects, leading to a strong electron-withdrawing character. As the methylene groups in the dpym and dpyp ligands feature an electron-donor character caused by inductive effects, central atoms in the different ligands appear to be ranged for the electronic donation as follows: nitrogen, carbon, and phosphorus. This is in line with our previous observation in [Cu(IPr)(dpa)][PF6] derivatives, in which the more electron rich the dpa, the more blueshifted the emission wavelength peak [13c].

Entry	Complex[a]	Absorption[a]	Emission[d]						
		λ_{max} [nm]	λ_{em} [nm][e,f]	λ_{em} [nm][f]	$\Delta\lambda_{em}$ [eV]	ϕ_{em}[e]	τ_{em} [μs][f]	τ_{em} [μs][g]	k_r [10^4 s^{-1}][f]
1	1	260 (2.31), 315 (1.37)[b]	463	481	0.10	0.22	13	45	1.7
2	2	269 (1.34), 315 (0.27)[c]	473	483	0.12	0.15	6	32	2.5
3	3	265 (1.30), 305 (0.30)[c]	474	482	0.10	0.73	14	38	5.2
4	4	244 (1.77), 279 (1.46), 330 (0.44)[c]	503	519	0.10	0.86	13	87	6.6

Table 2: Photoluminescence data of **1**–**4**.
[a] In brackets, ϵ [10^4 L mol^{-1} cm^{-1}].
[b] In $CHCl_3$ solution.
[c] In CH_2Cl_2 solution.
[d] Powder.
[e] Error of 0.05.
[f] at 298 K.
[g] at 77 K.

To further confirm these results, the adiabatic $S_0 \rightarrow S_x$ vertical transitions were calculated within the time-dependent DFT (TD-DFT) framework (Figures S11–S15 in the Supporting Information). Such approach enables us to describe up to three main types of transitions, for which the contributions are i) MLCT, ii) intraligand (IL) π–π* transition, and iii) NHC-to-ligand charge transfer (NHC-CT; Table 3). As a matter of fact, both the nature and the energy of the electronic transitions are strongly dependent on the bridging atom of the bis-pyridyl ligand. For instance, the small decrease of the band intensity assigned to the MLCT transition is noted for complexes with lower π-conjugation over the bis-pyridyl moiety (i.e., lower oscillator strength, see Figures S11–S15 in the Supporting Information). Based on the calculations on $\mathbf{2}^+$ and $\mathbf{3\,a}^+$ and $\mathbf{3\,b}^+$, the bands located at 265 and 269 nm for **2** and **3** are assigned to a mixture of MLCT and NHC-CT, respectively, and the bands at 315 and 305 nm are assigned to pure MLCT. Interestingly, from the calculation on $\mathbf{4}^+$, the band at 279 nm involves two distinct types of transition, that is, IL(π–π*) transitions ($S_0 \rightarrow S_2$) and NHC-CT transitions ($S_0 \rightarrow S_3$). The former is redshifted with respect to $\mathbf{1}^+$ as the phenyl moiety increases the overall π-conjugation over the whole ligand (see the Supporting Information). The last band of **4** located at 244 nm is assigned to a pure IL(π–π*)-type transition (Figures S12–S15 in the Supporting Information).

Complex	Band	E [eV]	λ [nm]	Main MO contribution	Type
[Cu(Ipr)(dpa)]$^+$ (1^+)	I	4.26	291.3	H−2→L (58 %)	MLCT/IL(π–π*)
		4.36	284.3	H−2→L+1 (73 %)	MLCT/IL(π–π*)
	II	4.99	248.4	H−2→L+2 (72 %)	MLCT/IL(π–π*)
[Cu(Ipr)(dpym)]$^+$ (2^+)	I	3.72	333.2	H−1→L (93 %)	MLCT
	II	4.32	286.9	H−2→L (69 %)	(ML/NHC)-CT
[Cu(Ipr)(dpyp)]$^+$ (3 a^+)	I	3.80	326.3	H−1→L (93 %)	MLCT
	II	4.36	284.5	H−2→L (59 %)	(ML/NHC)-CT
[Cu(Ipr)(dpyp)]$^+$ (3 b^+)	I	3.87	320.7	H−1→L (96 %)	MLCT
	II	4.49	276.2	Complex	(ML/NHC)-CT
[Cu(Ipr)(PPhpy$_2$)]$^+$ (4^+)	I	3.80	326.5	H−1→L (88 %)	MLCT
	II	4.34	285.6	H−2→L (81 %)	IL(ν/π–π*)
		4.39	282.2	H−3→L (51 %)	NHC-CT
	III	5.13	241.9	H−2→L+4 (63 %)	IL(ν/π–π*)

Table 3: Calculated vertical transition energies (E), absorption wavelength (λ), and corresponding main MO description for each band.

Next, the impact of the bridging atom on the photoluminescence features of the complexes were investigated. All the complexes show a broad and featureless emission band, suggesting a charge-transfer nature for the emitting excited state. In addition, the emission maximum is redshifted for **2** (473 nm), **3** (474 nm), and **4** (503 nm) compared with that of **1** (463 nm; Table 2). Interestingly, all the complexes show redshifted emission at 77 K (Figure 4 and Table 2), pointing out a TADF emission mechanism, as widely described in the literature [4]. This was further confirmed by measuring the excited state lifetime (τ_{em}) of the emission at 77 K. Indeed, all τ_{em} increased by a factor of at least 2.7 (minimum factor calculated for **3**) going from room temperature to 77 K (Table 2). Such increase of τ_{em} resulted from a change in the nature of the emitting excited state from singlet to triplet. Then, the central substitution on the bis-pyridyl ligand and its ability to participate in the π-conjugation seems to not significantly modify the $\Delta\lambda_{em}$, that is, the difference of energy between the singlet and the triplet excited states affecting the TADF process (Table 2). This parameter has been calculated by monitoring the changes of τ_{em} as a function of the temperature (between 77 and 298 K), fitting them by using the same TADF model previously used [13c, 21].

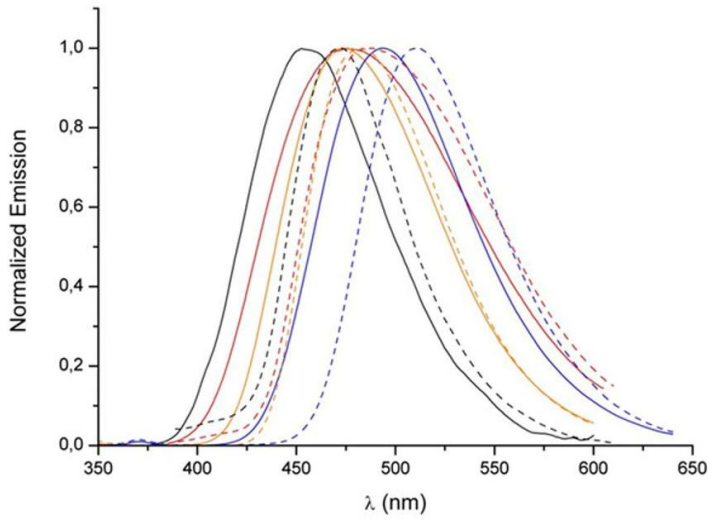

Figure 4: Photoluminescence spectra in the solid state (powder) at room temperature (solid line) and at 77 K (dotted line) of complexes **1** (black), **2** (red), **3** (orange), and **4** (blue).

Considering the direct fluorescence lifetimes, they were calculated as 670, 9.4, 141, and 101 ns for **1**, **2**, **3,** and **4**, respectively. The phosphorescence lifetimes were estimated at 45, 19.6, 37.1, and 86 μs for **1**, **2**, **3**, and **4**, respectively. As such, the $\Delta\lambda_{em}$ values were calculated as 0.095, 0.12, 0.10, and 0.10 eV for complexes **1**, **2**, **3**, and **4**, respectively (Figures S7–S9 and Tables S2–S4 in the Supporting Information).

Theoretical calculations further support these findings. In short, S_1 and T_1 were optimized by following the same approach as our previous study [13c], but at the PBE0/6–31+G(d,p)/SDD level of theory. This functional has been chosen for its capability to accurately describe intramolecular CT [22]. Estimated $\Delta\lambda_{em}$ values were in perfect agreement with those experimentally obtained (Tables 2 and 4). Likewise, calculated $S_1 \rightarrow S_0$ vertical energies that correspond to the fluorescence process were in good agreement with the experimental observation at 298 K, given the spectroscopic accuracy of TD-DFT calculations.

Complex	$E_{vert}^{S_1 \rightarrow S_0}$	$E_{vert}^{T_1 \rightarrow S_0}$	$\Delta E^{S/T}$
	[eV]	[eV]	Theo. [eV]
$[Cu(Ipr)(dpa)]^+$ (1^+)	2.40	2.19	0.08
$[Cu(Ipr)(dpym)]^+$ (2^+)	2.40	2.10	0.07
$[Cu(Ipr)(dpyp)]^+$ ($3\,a^+$)	2.45	2.14	0.09
$[Cu(Ipr)(dpyp)]^+$ ($3\,b^+$)	2.46	2.14	0.10
$[Cu(Ipr)(PPhpy_2)]^+$ (4^+)	2.34	2.09	0.06

Table 4: Calculated vertical $S_1 \rightarrow S_0$, $T_1 \rightarrow S_0$ emission energies (in eV). The theoretically estimated and experimental singlet–triplet energy splittings are also provided.

The rationalization of τ_{em} at 298 K is a challenging task, as it depends on collective properties, namely i) singlet–triplet energy splitting, ii) triplet state stability, and iii) geometrical deformations between T_1 and S_1; the lower the S_1/T_1 geometrical deformation, the faster the back-intersystem crossing (ISC) process, and the lower the τ_{em}. Complexes exhibit singlet–triplet splitting in the same range, which is in good agreement with experimental data (i.e., ca. 0.10 eV, Table 4). The lower τ_{em} value of **2** might be explained by i) a slightly less stable triplet state associated with a larger Cu atom spin density ($|\alpha_{Cu}>$=0.88 found for $\mathbf{2}^+$, see Figure 5) and ii) a smaller deviation of both folding and rotation parameters between S_1 and T_1 geometries (Figure S17 in the Supporting Information). In addition, the triplet stability improves by increasing the π-conjugation ($|\alpha_{Cu}>$ being 0.73 and 0.67 in $\mathbf{1}^+$ and $\mathbf{4}^+$, respectively).

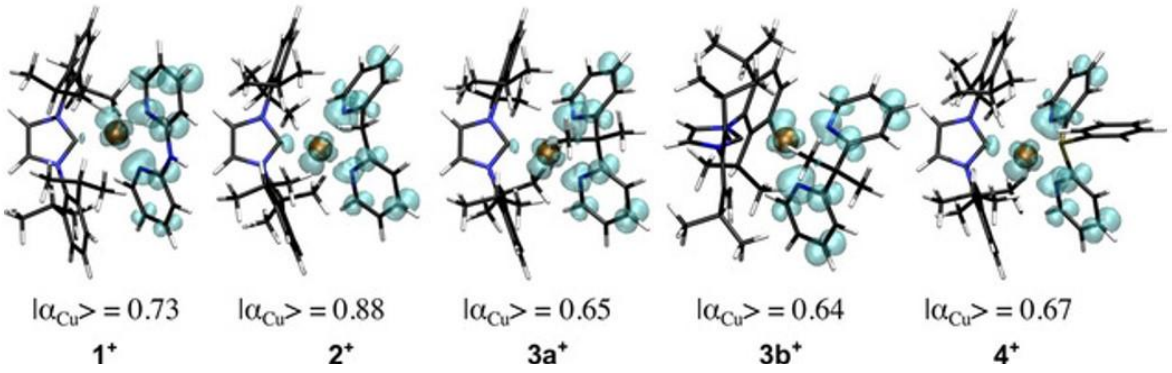

Figure 5: Triplet spin density plots of complexes $[Cu(IPr)(dpa)]^+$ ($\mathbf{2}^+$), $[Cu(IPr)(dpym)]^+$ ($\mathbf{3\,a}^+$), $[Cu(IPr)(dpyp)]^+$ ($\mathbf{3\,b}^+$), and $[Cu(IPr)(PPhpy_2)]^+$ ($\mathbf{4}^+$) (isovalues: 0.005 e a_0^{-3}).

In agreement with our previous study, both the rotation of the bis-pyridyl ligand with respect to the C_{NHC}–Cu^{I} bond and the folding of the bis-pyridyl ligand (Figure S17 in the Supporting Information) seem to play a key role in the kinetics of the back-ISC event. The presence of bulky moieties (e.g., methyl or phenyl moieties, respectively in **3** and **4**) is associated with i) a stronger deformation and ii) a lower flexibility of the bis-pyridyl ligand, which might explain longer excited state lifetime values, suggesting a strong reduction of the non-radiative decay process.

Although, the bridging atom does not substantially affect the TADF emission mechanism in this family of compounds, there is a strong enhancement of the ϕ_{em} values upon comparing **1** and **2** with **3** and **4** (i.e., 0.15, 0.22, 0.76, 0.86, respectively, Table 2). For instance, the addition of two methyl substituents at the bridging atom (**2** vs. **3**) leads to a more important symmetry breaking generated by a higher value of the plane angle θ (24.000(151)° in **2** vs. 29.886(96)° in **3 a**), the more pronounced pyramidal geometry of the bridging atom (57.352(229)° in **2** vs. 63.48(18)° in **3 a**), and the presence of the twisted conformer **3 b** leads to enhanced photoluminescence (ϕ_{em}=0.15 for **2** vs. ϕ_{em}=0.73 for **3**). Following this rationale, a very high ϕ_{em} of 0.86 was measured for **4**. Here, the plane angle θ and the pyramidal geometry of the phosphorus atom are more pronounced with respect to that of **3** (Figure 2). Finally, $\mathbf{1}^{+}$ exhibits the strongest geometry deformation between both S_1 and T_1 states. The planarity related to the π-conjugation over the ligand decreases the flexibility of bridged bis-pyridyl derivatives' dihedral angles. This results in an easier recombination from T_1 to S_1 excited states, as the ligand just has to rotate around C_{NHC}–Cu^{I} bond contrary to other complexes with a more pyramidal bridging atom, that is, a carbon or phosphorus atom. Flexibility is also likely involved for explaining the ϕ_{em} trends. The higher the flexibility, the lower the barrier for the non-radiative recombination to the S_0 state, explaining the lower ϕ_{em} of **1** and **2**. Geometry-dependent TADF was assessed by calculating the singlet–triplet splitting on both $\mathbf{3\,a}^{+}$ and $\mathbf{3\,b}^{+}$ conformers. The role of N^1-C^1···X-C^2 in the TADF is still under debate, as it has been shown to decrease TADF occurrence in boron-based dpa ligands [14b], but not in bidentate phenanthroline ones [23]. Our findings agree with the latter, two conformations exhibiting similar singlet–triplet splitting (0.09 and 0.10 eV, respectively, for conformations a and b, Table 4). This confirms the importance of both i) ligand flexibility and ii) S_1/T_1 geometry deformation rather than the orientation itself. The dpyp ligand can swap from T_1 to S_1 independently of its orientation contrary to the neutral boron-based dpa ligand. In a nutshell, our joint photophysical and theoretical study highlights that the replacement of the nitrogen atom by more pyramidal atoms significantly enhances the radiative deactivation pathway from the singlet excited state without affecting the TADF mechanism.

2.4 Electroluminescent study

Having rationalized the impact of the bridging atom on the photoluminescence features, we turned to investigate the electroluminescence behavior in a simple two-layer LEC device. In short, a 90 nm active layer consisting of the copper(I) complexes was deposited onto a indium–tin oxide (ITO) electrode coated with a 70 nm poly(3,4-ethylenedioxythiophene)/polystyrene sulfonate (PEDOT:PSS) layer. To finalize the device, a 90 nm aluminium cathode was evaporated. To provide a direct comparison between complexes, the devices were tested using a driving scheme based on a pulsed-current block wave at 1 kHz and a duty cycle of 50 % (Figure S18 in the Supporting Information).

However, as previously noted for LECs based on **1 [13c]**, the color stability is significantly compromised upon using high pulsed currents owing to the prominent degradation of the emitter. High pulsed currents of around 50 mA are necessary to inject enough charges to reach a light output superior to 1 cd m^{-2}. This makes these devices very inefficient with an efficacy value of around 4×10^{-3} cd A^{-1}. To shed light onto the poor charge injection mechanism, we determined the ionic conductivity (σ) by using the electrochemical impedance spectroscopy technique (see the Experimental Section). This parameter affects the formation of electrical double layers (EDLs), which assist charge injection in LECs [24]. In detail, devices with **3** and **4** feature similar σ values of 8×10^{-8} and 6×10^{-8} S m^{-1}, respectively. Both values significantly contrast with that of devices with **2** (4×10^{-9} S m^{-1}), whereas the σ value of devices with **1** could not be determined with enough accuracy owing to the high resistance value. Quite likely, the enhanced ionic mobility features of **3** and **4** should be related to the distorted geometry caused by the bridging atom, which reduces the cation ion binding energy ($E_{c\text{-}a}$). In other words, devices with **3** and **4** should easily form EDLs, allowing us to apply low currents, whereas **1**

and **2** should not show any electroluminescence response. Both, σ and ϕ_{em} parameters, prompt a significant enhancement of the device efficiency upon changing the bridging atom going from **1** and **2** to **3** and **4**.

To confirm this notion, all of the devices were driven at different pulsed currents from 0.5 to 5 mA. At the lowest applied current (Figure 6 and Table 5), devices with **3** and **4** feature an almost instantaneous electroluminescence response, achieving luminance and efficacy values up to 6.2 cd m^{-2} and 0.19 cd A^{-1} and up to 13.0 cd m^{-2} and 0.39 cd A^{-1}, respectively. As expected, devices with **1** and **2** showed neither an electrical response nor light output. The latter showed an electroluminescence behavior at applied currents of 5 mA, reaching luminance and efficacy values of around 2 cd m^{-2} and 1×10^{-2} cd A^{-1}, respectively (Table 5 and Figure S18 in the Supporting Information). Notably, the luminance (30 cd m^{-2}) and efficacy (0.15 cd A^{-1}) of devices with **4** hold upon using 5 mA pulsed currents (Table 5).

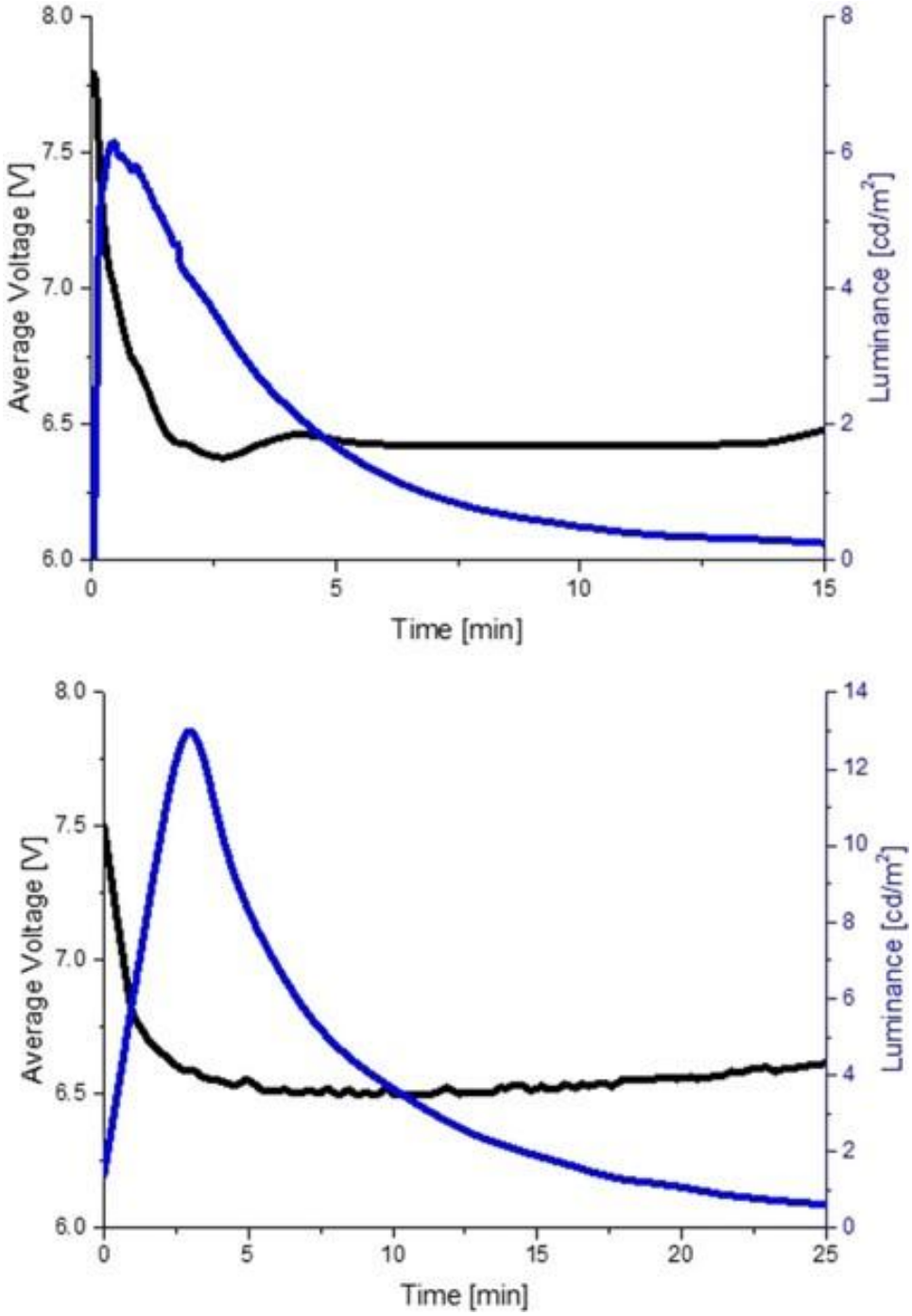

Figure 6: Luminance and average voltage versus time of devices prepared with **3** (top) and **4** (bottom) driven at 0.5 mA pulsed mode with a block wave form at 1 kHz and a duty cycle of 50 %.

Complex	Electroluminescence			
	I_{avg} [mA]	Lum. [cd m^{-2}][a]	Efficacy [cd A^{-1}]	$t_{1/2}$ [s][b]
1	5	2.6	0.007	44
2	5	2.2	0.001	36
3	0.5	6.2	0.19	240
	5	21.5	0.067	324
4	0.5	13	0.39	42
	5	32	0.10	10

Table 5: Figures of merit for devices prepared with **1**–**4** driven at different pulsed currents (I_{avg}).
[a] Lum. corresponds to the maximum luminance value.
[b] $t_{1/2}$ is the time to reach half of the maximum luminance.

This significant improvement might be solely ascribed to the enhancement of both σ and ϕ_{em} upon only changing the bridging atom of the bis-pyridyl ligand. Indeed, under the above-mentioned driving conditions, devices show a similar mechanism as derived from the average voltage profile, that is, an immediately drop to a plateau owing to the formation of the EDLs and a slow increase caused by the degradation of the active layer. As far as the decay of the luminescence is concerned, this might be related to the quenching of the emission by the approaching of the p- and n-doped regions, reducing the thickness of the emitting junction. Finally, changes in the electroluminescence spectrum were not noted under device operation conditions, showing a light blue (**1** and **2**), blue (**2**), greenish blue (**3**), and dark green (**4**) emission with *x*/*y* color coordinates of 0.23/0.28, 0.30/0.42, 0.23/0.39, and 0.31/0.51, respectively.

3 Experimental Section

3.1 General considerations

All reactions were carried out by using standard Schlenk techniques under an atmosphere of dry argon. Solvents were purchased from Carlo Erba and degassed prior to use by bubbling argon gas directly into the solvent. Solvents for NMR spectroscopy were dried over molecular sieves. NMR spectra were recorded with 400 MHz and 500 MHz Brucker spectrometers. Proton (^{1}H) NMR information is given in the following format: multiplicity (s, singlet; d, doublet; t, triplet; q, quartet; qui, quintet; sex, sextet; sept, septet; m, multiplet), coupling constant(s) (*J*) in Hertz (Hz), number of protons. The prefix app is occasionally applied when the true signal multiplicity was unresolved and br indicates the signal in question is broadened. Carbon (^{13}C) NMR spectra are reported in ppm (δ) relative to residual $CHCl_3$ (δ=77.0 ppm) unless noted otherwise and information on carbon multiplicity is given in the following format: multiplicity (s, singlet for C; d, doublet for CH; t, triplet for CH_2; and q, quartet for CH_3). The full signals attributions are given in the Supporting Information, as well as a copy of the NMR spectra. HRMS were performed by LCMT analytical services. NMR solvents were passed through a pad of basic alumina before use. 2,2′-Dipyridylamine was purchased from Sigma–Aldrich and used without prior purification. The copper complexes [CuCl(IPr)] [25] and [CuOH(IPr)] [26] were synthesized by following reported procedures.

3.2 Synthesis of complex 2

In a flame-dried Schlenk tube under an argon atmosphere, [CuCl(IPr)] complex (150 mg, 0.30 mmol) and ligand dpym (55 mg, 0.32 mmol) were dissolved in degassed absolute ethanol (7.5 mL) and heated under reflux for 1 h. After cooling the reaction mixture to room temperature, an aqueous

solution of KPF_6 (166 mg, 0.9 mmol in around 5 mL of water) was added, affording a white precipitate. The solid was collected on a frit, washed with water, and dried under air and then under vacuum. The copper complex [Cu(IPr)(dpym)][PF_6] (**2**) was obtained as a light-brown powder (220 mg, 0.29 mmol, 96 % yield). ^{1}H NMR ($CDCl_3$, 400 MHz): δ=1.11 (d, J=6.8 Hz, 12 H), 1.23 (d, J=6.8 Hz, 12 H), 2.72 (sept, J=6.8 Hz), 3.88 (s, 2 H), 6.89–6.93 (m, 4 H), 7.27–7.32 (m, 6 H), 7.48–7.53 (m, 4 H), 7.67 ppm (dt, J=1.6, 7.6 Hz, 2 H); ^{13}C NMR ($CDCl_3$, 100 MHz): δ=24.0 (q, ×4), 24.2 (q, ×4), 28.8 (d, ×4), 43.6 (t), 122.8 (d, ×2), 123.5 (d, ×2), 124.4 (d, ×4), 125.5 (d, ×2), 130.6 (d, ×2), 135.8 (s, ×2), 139.3 (d, ×2), 145.8 (s, ×4), 148.9 (d, ×2), 154.6 (s, ×2), 183.6 ppm (s); IR (neat): ν=2965, 1600, 1573, 1471, 1443, 836 cm^{-1}; HRMS (ESI): m/z calcd for $C_{38}H_{46}N_4Cu$ [M−PF_6]$^+$: 621.3018; found: 621.3040.

3.3 Synthesis of complex 3

In a flame-dried Schlenk tube under an argon atmosphere, [CuOH(IPr)] complex (234.6 mg, 0.5 mmol) and 2,2′-dipyridyl-2,2-propane (dpyp; 99.1 mg, 0.5 mmol) were dissolved in dry degassed toluene. HBF_4·Et_2O (68 µL, 0.5 mmol) was added dropwise and the reaction mixture was stirred overnight at room temperature. Pentane was added, affording a white precipitate, which was collected on a frit, washed with pentane, and dried under vacuum. Then, in a round-bottom flask, the [Cu(IPr)(dpyp)][BF_4] complex and KPF_6 (304 mg, 1.65 mmol) were dissolved in MeOH. The mixture was stirred for 1 h at room temperature and then concentrated to dryness. The crude mixture was dissolved in dichloromethane, filtered through a pad of Celite®, and concentrated under vacuum, leading to the pure copper complex [Cu(IPr)(dpyp)][PF_6] (**3**) as a white-yellowish powder (237 mg, 0.30 mmol, 59 % yield). ^{1}H NMR ($CDCl_3$, 400 MHz): δ=1.12 (d, J=6.8 Hz, 12 H), 1.24 (d, J=6.8 Hz, 12 H), 1.69 (s, 6 H), 2.80 (sept, J=6.8 Hz, 4 H), 6.95 (m, 2 H), 7.08 (d, J=4.3 Hz, 2 H), 7.32 (d, J=7.6 Hz, 4 H), 7.33 (s, 2 H), 7.50–7.57 (m, 4 H), 7.72 ppm (t, J=7.3 Hz, 2 H); ^{13}C NMR ($CDCl_3$, 100 MHz): δ=23.5 (q, ×4), 24.9 (q, ×4), 28.7 (d, ×4), 44.5 (s), 121.6 (d, ×2), 122.6 (d, ×2), 123.9 (d, ×2), 124.4 (d, ×4), 130.7 (d, ×2), 135.8 (s, ×2), 139.3 (d, ×2), 145.9 (s, ×4), 149.5 (d, ×2), 161.6 (s, ×2), 183.2 ppm (s); IR (neat): ν=1595, 1464, 1402, 1365, 1327, 1061, 838, 803, 761, 743 cm^{-1}; HRMS (ESI): m/z calcd for $C_{40}H_{50}N_4Cu$ [M−PF_6]$^+$: 649.3331; found: 649.3333.

3.4 Synthesis of complex 4

In a flame-dried Schlenk tube under an argon atmosphere, [CuOH(IPr)] complex (155 mg, 0.33 mmol) and bis(2-pyridyl)phenylphosphine ($PPhpy_2$; 87 mg, 0.33 mmol) were dissolved in dry degassed toluene. HBF_4·Et_2O (45 µL, 0.33 mmol) was added dropwise and the reaction mixture was stirred overnight at room temperature. Pentane was added, affording a white precipitate, which was collected on a frit, washed with pentane, and dried under vacuum. Then, in a round-bottom flask, the [Cu(IPr)($PPhpy_2$)][BF_4] complex and KPF_6 (304 mg, 1.65 mmol) were dissolved in MeOH. The mixture was stirred for 1 h at room temperature and then concentrated to dryness. The crude mixture was dissolved in dichloromethane, filtered through a pad of Celite®, and concentrated under vacuum, leading to the pure copper complex [Cu(IPr)($PPhpy_2$)][PF_6] (**4**) as a yellowish powder (205 mg, 0.24 mmol, 72 % yield). ^{1}H NMR ($CDCl_3$, 400 MHz): δ=1.16 (d, J=6.9 Hz, 12 H), 1.22 (d, J=6.9 Hz, 12 H), 2.76 (sept, J=6.9 Hz, 4 H), 6.96–6.99 (m, 4 H), 7.23–7.24 (m, 6 H), 7.31 (s, 2 H), 7.47 (t, J=7.8 Hz, 2 H), 7.53 (t, J=7.7 Hz, 2 H), 7.51–7.58 ppm (m, 5 H); ^{13}C NMR ($CDCl_3$, 100 MHz): δ=23.9 (q, ×4), 24.4 (q, ×4), 28.7 (d, ×4), 123.4 (d, ×2), 123.7 (d, ×2), 124.2 (d, ×4), 126.9 (d, ×2, appears as a d, $^2J_{C\text{-}P}$=9.4 Hz), 127.0 (s, appears as a d, $^1J_{C\text{-}P}$=24.5 Hz), 130.2 (d, ×2, appears as a d, $^2J_{C\text{-}P}$=9.7 Hz), 130.5 (d, ×2), 132.7 (d), 135.8 (s), 137.4 (d, ×2), 137.7 (d, ×2, appears as a d, $^2J_{C\text{-}P}$=24.6 Hz), 145.7 (s, ×4), 150.0 (d, ×2, appears as a d, $^4J_{C\text{-}P}$=7.8 Hz), 159.6 (s, ×2, appears as a d, $^1J_{C\text{-}P}$=5.1 Hz), 183.3 ppm (s); IR (neat): ν=2962, 1581, 1446, 1328, 1102, 835, 752 cm^{-1}; HRMS (ESI): m/z calcd for $C_{43}H_{49}N_4PCu$ [M−PF_6]$^+$: 715.2991; found: 715.3011.

3.5 Computational details

Geometries were optimized with the B3LYP functional in which the DFT-D3 dispersion correction [27] was included for a better description of long-range interactions such as CH–π interactions, respectively between the dpa and NHC ligands. The effective core potential SDD was used for the copper atom and the 6–31+G(d,p) basis set for carbon, nitrogen, hydrogen, phosphorus, and oxygen atoms. Recently, we have shown that charge-transfer states upon excitation play a crucial role in the

photophysical properties of $[Cu(NHC)(dpa)]^+$ complexes. Therefore, TD-DFT calculations were performed with the PBE0 functional, which has been shown to be particularly relevant to describe TADF events [22]. Both S_0–S_1 and S_0–T_1 transitions were considered and their natures were assigned by plotting the Natural Transition Orbital analysis, in which molecular orbital contributions to a given transition are summed and weighted according to their CI coefficients. TADF were calculated from both optimized S_1 and T_1 energies. The former was calculated by using the implemented TD-DFT gradients whereas the latter was obtained from open-spin-relaxed open shell calculations. Calculations were performed by using the Gaussian 09 Revision D.01 package [28]. Visualization were carried out with the VMD program [29].

3.6 Device preparation and analysis

Double layer LECs were fabricated as follows. ITO coated glass plates were patterned by conventional photolithography (Naranjo Substrates). The substrates were cleaned by using sequential ultrasonic baths, namely in water–soap, water, ethanol, and propan-2-ol solvents. After drying, the substrates were placed in a UV–ozone cleaner (Jetlight 42–220) for 8 min. A 100 nm layer of PEDOT:PSS was doctor-bladed onto the ITO glass substrate to increase the device preparation yield (400 μm substrate distance and a speed of 10 mm s^{-1}). The luminescent layer was entirely prepared with copper(I) complexes. The active layer was deposited by means of the doctor-blading technique (600 μm substrate distance and a speed of 20 mm s^{-1}) reaching a thickness of 90–100 nm. These conditions resulted in homogeneous thin films with a roughness less than 5 %, with no apparent optical defects. The latter was determined by using a profilometer DektakxT from Bruker. Once the active layer was deposited, the samples were transferred into an inert atmosphere glovebox (<0.1 ppm O_2 and H_2O, Innovative Technology). The aluminium cathode electrode (90 nm) was thermally evaporated by using a shadow mask under high vacuum (<1×10^{-6} mbar) from using an Angstrom Covap evaporator integrated into the inert atmosphere glovebox. The time dependence of the luminance, voltage, and current was measured by applying constant and/or pulsed voltage and current by monitoring the desired parameters simultaneously by using an Avantes spectrophotometer (Avaspec-ULS2048L-USB2) in conjunction with a calibrated integrated sphere Avasphere 30-Irrad and Botest OLT OLED Lifetime-Test System. Electroluminescence spectra were recorded by using the same spectrophotometer. Electrochemical impedance spectroscopic assays were carried out with a potentiostat/galvanostat (PGSTAT30, Autolab) equipped with a frequency response analyzer module (FRA). Measurements were performed at the applied voltage of 0 V after a LIV sweep from 0 to 7 V. The AC signal amplitude was set to 50 mV, modulated in a frequency range from 1 to 10^6 Hz. The Nova 1.11 software was used to obtain the parameters from the *R*−*R*/*C* equivalent circuit.

4 Conclusion

This work demonstrates, with the support of both experimental and theoretical studies, that the nature of the bridging atom between the two coordinating pyridine rings plays an important role on the photo- and electroluminescent properties of NHC copper(I) complexes. Indeed, the molecular distortion is a key parameter to design new complexes for lighting applications. This work discloses that moving from a planar-like structure (X is NH (**1**) and CH_2 (**2**)) to a boat-like structure (X is $C(CH_3)_2$ (**3**) and PPh (**4**)) of the bis-pyridyl ligand significantly enhances the ϕ_{em} without affecting the TADF mechanism. In addition, this distortion strongly increases the σ of thin films, leading to the easy formation of EDLs under low applied currents. As such, devices with the new complexes **3** and **4** outperformed the current state-of-the-art in LECs based on NHC copper(I) complexes. Here, moderate luminance (10–15 cd m^{-2}) and efficacy (0.2–0.4 cd A^{-1}) values were reached under applied low currents (0.5 mA). Noteworthy, these features hold upon increasing the applied currents up to 5 mA, outperforming devices prepared with the archetypal complex **1** with luminance (3 cd m^{-2}) and efficacy (7×10^{-3} cd A^{-1}). Overall, this work provides key information on enhancing both the photo- and electroluminescent features of an emerging family of copper(I) complexes.

Acknowledgements

This work was supported by the "Ministère de la Recherche et des Nouvelles Technologies", CNRS (Centre National de la Recherche Scientifique) and the LABEX SynOrg (ANR-11-LABX-0029). We thank the "Agence Nationale de la Recherche", within the CSOSG program (ANR-12-SECU-0002-02), the ANR program (ANR-15-CE39-0006), and the "Région Basse-Normandie" for their funding (F.S. and M.E.). M.L. acknowledges SeRC (Swedish e-Science Research Center) for funding. F.D.M. thanks the Swedish Research Council (Grant No. 621–2014–4646). F.D.M. and M.L. acknowledge SNIC (Swedish National Infrastructure for Computing) for providing computer resources (snic001-12–192). R.D.C. and M.D.W. acknowledge the support by the 'Fonds der Chemischen Industrie" (FCI) in the Liebig grant framework. R.D.C. further acknowledges the program "Ayudas para la atracción de talento investigador–Modalidad 1 of the Consejería de Educación, Juventud *y* Deporte–Comunidad de Madrid with the reference number 2016-T1/IND-1463". F.D.M. and M.L. are grateful to Prof. J. C. Sancho-García for his generous support. S.G. thanks Johnson Matthey for the gift of metals.

Conflict of interest

The authors declare no conflict of interest.

Keywords

Copper(I) complexes, density functional theory, light-emitting electrochemical cells, photoluminescence, thermally activated delayed fluorescence

References

[1a] R. D. Costa, E. Ortí, H. J. Bolink, F. Monti, G. Accorsi, N. Armaroli, *Angew. Chem. Int. Ed.* 2012, 51, 8178– 8211; *Angew. Chem.* 2012, 124, 8300– 8334;

[1b] S. B. Meier, D. Tordera, A. Pertegás, C. Roldán-Carmona, E. Ortí, H. J. Bolink, *Mater. Today* 2014, 17, 217– 223;

[1c] Z. Yu, L. Li, H. Gao, Q. Pei, *Sci. China Chem.* 2013, 56, 1075– 1086;

[1d] E. Fresta, R. D. Costa, *J. Mater. Chem. C* 2017, 5, 5643– 5675.

[2a] Y.-M. Wang, F. Peng, Y.-B. Hou, Z. Xu, Y.-S. Wang, W.-F. Fu, *Appl. Phys. Lett.* 2005, 87, 233512;

[2b] N. Armaroli, G. Accorsi, M. Holler, O. Moudam, J.-F. Nierengarten, Z. Zhou, R. T. Wegh, R. Welter, *Adv. Mater.* 2006, 18, 1313– 1316;

[2c] R. D. Costa, D. Tordera, E. Ortí, H. J. Bolink, J. Schönle, S. Graber, C. E. Housecroft, E. C. Constable, J. A. Zampese, *J. Mater. Chem.* 2011, 21, 16108– 16118;

[2d] S. Keller, E. C. Constable, C. E. Housecroft, M. Neuburger, A. Prescimone, G. Longo, A. Pertegás, M. Sessolo, H. J. Bolink, *Dalton Trans.* 2014, 43, 16593– 16596;

[2e] C. Bizzarri, C. Strabler, J. Prock, B. Trettenbrein, M. Ruggenthaler, C.-H. Yang, F. Polo, A. Iordache, P. Brüggeller, L. D. de Cola, *Inorg. Chem.* 2014, 53, 10944– 10951;

[2f] F. Brunner, L. Martinez-Sarti, S. Keller, A. Pertegás, A. Prescimone, E. C. Constable, H. J. Bolink, C. E. Housecroft, *Dalton Trans.* 2016, 45, 15180– 15192;

[2g] S. Keller, A. Pertegás, G. Longo, L. Martinez, J. Cerdá, J. M. Junquera-Hernández, A. Prescimone, E. C. Constable, C. E. Housecroft, E. Ortí, H. J. Bolink, *J. Mater. Chem. C* 2016, 4, 3857– 3871.

[3a] D. Volz, M. Wallesch, C. Fléchon, M. Danz, A. Verma, J. M. Navarro, D. M. Zink, S. Bräse, T. Baumann, *Green Chem.* 2015, 17, 1988– 2011;

[3b] E. Cariati, E. Lucenti, C. Botta, U. Giovanella, D. Marinotto, S. Righetto, *Coord. Chem. Rev.* 2016, 306, 566– 614.

[4a] H. Uoyama, K. Goushi, K. Shizu, H. Nomura, C. Adachi, *Nature* 2012, 492, 234– 238;

[4b] Y. Tao, K. Yuan, P. Xu, H. Li, R. Chen, C. Zheng, L. Zhang, W. Huang, *Adv. Mater.* 2014, 26, 7931– 7958;

[4c] R. Czerwieniec, M. J. Leitl, H. H. H. Homeir, H. Yersin, *Coord. Chem. Rev.* 2016, 325, 2– 28;

[4d] L. Bergmann, G. J. Hedley, T. Baumann, S. Bräse, I. D. W. Samuel, *Sci. Adv.* 2016, 2, e 1500889.

[5] G. Blasse, D. R. McMillin, *Chem. Phys. Lett.* 1980, 70, 1– 3.

[6a] D. R. McMillin, K. M. McNett, *Chem. Rev.* 1998, 98, 1201– 1220;

[6b] C. T. Cunningham, J. J. Moore, K. L. H. Cunningham, P. E. Fanwick, D. R. McMillin, *Inorg. Chem.* 2000, 39, 3638– 3644;

[6c] M. Iwamura, S. Takeuchi, T. Tahara, *Acc. Chem. Res.* 2015, 48, 782– 791;

[6d] M. W. Mara, K. A. Fransted, L. X. Chen, *Coord. Chem. Rev.* 2015, 282–283, 2– 18.

[7] A. Kaeser, M. Mohankumar, J. Mohanraj, F. Monti, M. Holler, J.-J. Cid, O. Moudam, I. Nierengarten, L. Karmazin-Brelot, C. Duhayon, B. Delavaux-Nicot, N. Armaroli, J.-F. Nierengarten, *Inorg. Chem.* 2013, 52, 12140– 12151.

[8] T. Gneuß, M. J. Leitl, L. H. Finger, H. Yersin, J. Sundermeyer, *Dalton Trans.* 2015, 44, 20045– 20055.

[9] Z.-C. Fu, Q. Yin, Z.-F. Yao, C. Li, W.-F. Fu, *J. Coord. Chem.* 2015, 68, 3282– 3294.

[10] J.-L. Chen, Z.-H. Guo, H.-G. Yu, L.-H. He, S.-J. Liu, H.-R. Wen, J.-Y. Wang, *Dalton Trans.* 2016, 45, 696– 705.

[11] R. Visbal, M. C. Gimeno, *Chem. Soc. Rev.* 2014, 43, 3551– 3574.

[12a] K. Matsumoto, N. Matsumoto, A. Ishii, T. Tsukuda, M. Hasegawa, T. Tsubomura, *Dalton Trans.* 2009, 6795– 6801;

[12b] V. A. Krylova, P. I. Djurovich, M. T. Whited, M. E. Thompson, *Chem. Commun.* 2010, 46, 6696– 6698;

[12c] V. J. Catalano, L. B. Munro, C. E. Strasser, A. F. Samin, *Inorg. Chem.* 2011, 50, 8465– 8476;

[12d] V. A. Krylova, P. I. Djurovich, J. W. Aronson, R. Haiges, M. T. Whited, M. E. Thompson, *Organometallics* 2012, 31, 7983– 7993;

[12e] P. Ai, M. Mauro, L. De Cola, A. A. Danopoulos, P. Braunstein, *Angew. Chem. Int. Ed.* 2016, 55, 3338– 3341; *Angew. Chem.* 2016, 128, 3399– 3402;

[12f] Z. Wang, C. Zheng, W. Wang, C. Xu, B. Ji, X. Zhang, *Inorg. Chem.* 2016, 55, 2157– 2164;

[12g] R. Molteni, K. Edkins, M. Haenel, A. Steffen, *Organometallics* 2016, 35, 629– 640;

[12h] M. Nishikawa, T. Sano, M. Washimi, K. Takao, T. Tsubomura, *Dalton Trans.* 2016, 45, 12127– 12136;

[12i] S. Shi, L. R. Collins, M. F. Mahon, P. I. Djurovich, M. E. Thompson, M. K. Whittlesey, *Dalton Trans.* 2017, 46, 745– 752.

[13a] R. Marion, F. Sguerra, F. Di Meo, E. Sauvageot, J.-F. Lohier, R. Daniellou, J.-L. Renaud, M. Linares, M. Hamel, S. Gaillard, *Inorg. Chem.* 2014, 53, 9181– 9191;

[13b] R. Marion, F. Sguerra, F. Di Meo, E. Sauvageot, J.-F. Lohier, R. Daniellou, J.-L. Renaud, M. Linares, M. Hamel, S. Gaillard, *Inorg. Chem.* 2016, 55, 4068;

[13c] M. Elie, F. Sguerra, F. Di Meo, M. D. Weber, R. Marion, A. Grimault, J.-F. Lohier, A. Stallivieri, A. Brosseau, R. B. Pansu, J.-L. Renaud, M. Linares, M. Hamel, R. D. Costa, S. Gaillard, *ACS Appl. Mater. Interfaces* 2016, 8, 14678– 14691.

[14a] V. A. Krylova, P. I. Djurovich, B. L. Conley, R. Haiges, M. T. Whited, T. J. Williams, M. E. Thompson, *Chem. Commun.* 2014, 50, 7176– 7179;

[14b] M. J. Leitl, V. A. Krylova, P. I. Djurovitch, M. E. Thompson, H. Yersin, *J. Am. Chem. Soc.* 2014, 136, 16032– 16038.

[15] T. L. Davis, J. L. Watts, K. J. Brown, J. S. Hewage, A. R. Treleven, S. V. Lindeman, J. R. Gardinier, *Dalton Trans.* 2015, 44, 15408– 15412.

[16] G. Dyker, O. Muth, *Eur. J. Org. Chem.* 2004, 4319– 4322.

[17] N. Vedernikov, R. Miftakhov, S. V. Borisoglebski, K. G. Caulton, B. N. Solomonov, *Chem. Heterocyclic Comp.* 2002, 38, 406– 416.

[18] S. A. Saucedo Anaya, A. Hagenbach, U. Abram, *Polyhedron* 2008, 27, 3587– 3592.

[19a] A. Kobayashi, T. Hasegawa, M. Yoshida, M. Kato, *Inorg. Chem.* 2016, 55, 1978– 1985;

[19b] S. Hanf, R. Garcia-Rodriguez, S. Feldmann, A. D. Bond, E. Hey-Hawkins, D. S. Wright, *Dalton Trans.* 2017, 46, 814– 824.

[20] M. E. Jung, G. Piizzi, *Chem. Rev.* 2005, 105, 1735– 1766.

[21] J. Nitsch, F. Lacemon, A. Lorbach, A. Eichhorn, F. Cisnetti, A. Steffen, *Chem. Commun.* 2016, 52, 2932– 2935.

[22] M. Moral, L. Muccioli, W.-J. Son, Y. Olivier, J.-C. Sancho-García, *J. Chem. Theory Comput.* 2015, 11, 168– 177.

[23] J. Föller, M. Kleinschmidt, C. M. Marian, *Inorg. Chem.* 2016, 55, 7508– 7516.

[24a] B. M. D. Puscher, M. F. Aygüler, P. Docampo, R. D. Costa, *Adv. Energy Mater.* 2017, 7, 1602283;

[24b] M. D. Weber, J. E. Wittmann, A. Burger, O. B. Malcioğlu, J. Segarra-Martí, A. Hirsch, P. B. Coto, M. Bockstedte, R. D. Costa, *Adv. Funct. Mater.* 2016, 26, 6737– 6750;

[24c] L. D. Bastatas, K.-Y. Lin, M. D. Moore, K. J. Suhr, M. H. Bowler, Y. Shen, B. J. Holliday, J. D. Slinker, *Langmuir* 2016, 32, 9468– 9474;

[24d] A. Munar, A. Sandström, S. Tang, L. Edman, *Adv. Funct. Mater.* 2012, 22, 1511– 1517.

[25] C. A. Citadelle, E. Le Nouy, F. Bisaro, A. M. Z. Slawin, C. S. J. Cazin, *Dalton Trans.* 2010, 39, 4489– 4491.

[26] G. C. Fortman, A. M. Z. Slawin, S. P. Nolan, *Organometallics* 2010, 29, 3966– 3972.

[27a] S. Grimme, J. Antony, S. Ehrlich, H. Krieg, *J. Chem. Phys.* 2010, 132, 154104;

[27b] S. Grimme, S. Ehrlich, L. Goerigk, *J. Comput. Chem.* 2011, 32, 1456– 1465.

[28] Gaussian 09, Revision D.02, M. J. Frisch, G. W. Trucks, H. B. Schlegel, G. E. Scuseria, M. A. Robb, J. R. Cheeseman, G. Scalmani, V. Barone, G. A. Petersson, H. Nakatsuji, X. Li, M. Caricato, A. Marenich, J. Bloino, B. G. Janesko, R. Gomperts, B. Mennucci, H. P. Hratchian, J. V. Ortiz, A. F. Izmaylov, J. L. Sonnenberg, D. Williams-Young, F. Ding, F. Lipparini, F. Egidi, J. Goings, B. Peng, A. Petrone, T. Henderson, D. Ranasinghe, V. G. Zakrzewski, J. Gao, N. Rega, G. Zheng, W. Liang, M. Hada, M. Ehara, K. Toyota, R. Fukuda, J. Hasegawa, M. Ishida, T. Nakajima, Y. Honda, O. Kitao, H. Nakai, T. Vreven, K. Throssell, J. A. Montgomery, Jr., J. E. Peralta, F. Ogliaro, M. Bearpark, J. J. Heyd, E. Brothers, K. N. Kudin, V. N. Staroverov, T. Keith, R. Kobayashi, J. Normand, K. Raghavachari, A. Rendell, J. C. Burant, S. S. Iyengar, J. Tomasi, M. Cossi, J. M. Millam, M. Klene, C. Adamo, R. Cammi, J. W. Ochterski, R. L.

Martin, K. Morokuma, O. Farkas, J. B. Foresman, D. J. Fox, Gaussian, Inc., Wallingford CT, **2016**.

[29] W. Humphrey, A. Dalke, K. Schulten, *J. Mol. Graphics* 1996, 14, 33– 38